Biosensors and Bioelectronics 183 (2021) 113201

Contents lists available at ScienceDirect

Biosensors and Bioelectronics

journal homepage: http://www.elsevier.com/locate/bios

Short communication

Flexible triphase enzyme electrode based on hydrophobic porous PVDF membrane for high-performance bioassays

Haili Wang, Jun Zhang **, Dandan Wang, Zhaohong Wang, Yangru Chen, Xinjian Feng *

College of Chemistry, Chemical Engineering and Materials Science, Soochow University, Suzhou, 215123, PR China

ARTICLE INFO

Keywords:
Hydrophobicity
Triphase interface
Oxidase kinetics
Flexible biosensor

ABSTRACT

Flexible bioassays based on oxidase-catalyzed and electrocatalytic cascade reactions have been widely reported. However, the fluctuant oxygen level and high anodic potential restricts the detection accuracy. To overcome these challenges, we report here a flexible triphase enzyme electrode by assembling an oxidase enzyme layer and Pt electrocatalysts onto a carbon nanotube film/porous polyvinylidene fluoride hydrophobic substrate. Such a flexible enzyme electrode has an air-liquid-solid triphase reaction zone where oxygen level is air phase dependent (constant and sufficient high), which stabilized the oxidase kinetics and enabled the cathodic measurement of enzymatic product H_2O_2 with minimum interferents caused from oxygen level fluctuation and many oxidizable species in analyte solution. Furthermore, the flexible triphase enzyme electrode exhibited good mechanical stability even after being bent over 600 times and an excellent air permeability, which are crucial to wearable devices that require long-term skin contact.

1. Introduction

Flexible biosensors have attracted great attention in recent years with the rapid development of wearable electronics and the increasing emphasis on non-invasive detection of individual's physiological biomarkers for real-time health status monitoring (Lee et al., 2020; Yang and Gao. 2019; Kim et al., 2019; Yoon et al., 2019; Gao et al., 2016; Imani et al., 2016; Yao et al., 2011). Electrochemical biosensing based on bio-electrochemical cascade reactions between the specific oxidase catalysis ($R + O_2 \xrightarrow{Ox} P + H_2O_2$) and the electrochemical oxidation ($H_2O_2 \rightarrow O_2 + 2H^+ + 2e^-$) has been widely studied in bioelectronic devices since 1973 (Guilbault and Lubrano. 1973; Wilson and Hu. 2000; Chen et al., 2015; Li et al., 2015; Kim et al., 2017; Zhang et al., 2020). However, fluctuating oxygen concentration in biofluids affects the oxidase kinetics and the formation rate of H_2O_2; the electro-oxidation of H_2O_2 requires a relatively high potential (e.g., 0.6–0.7 V at Pt) at which the amount of interferents in biofluids can also be oxidized (Evans et al., 2002; Hrapovic et al., 2004; Lad et al., 2014; Kim et al., 2018; Kumar et al., 2018). These two species generally lead to the low detection accuracy.

Interfacial microenvironments that govern mass and electron transport are of great importance to the electrochemical oxidations that occur at the electrode/electrolyte interface (Zhan et al., 2018; Song et al., 2018; Mi et al., 2017; Lu et al., 2016; Lei et al., 2016). Superhydrophobic surfaces have recently received substantial interest and show great potential in many fields, such as heat transfer (Li et al., 2016), drug release (Yohe et al., 2012), photocatalysis (Sheng et al., 2017; Zhou et al., 2020), self-cleaning (Lu et al., 2015), and material electrodeposition (Zhang et al., 2017; Wang et al., 2014). When a superhydrophobic substrate is in contact with an aqueous solution, it can trap air pockets inside the porous structure, leading to the formation of an air-liquid-solid triphase interfacial microenvironment where oxygen will be directly obtained through and from the gas phase (constant and sufficient) (Barthlott and Neinhuis. 1997; Feng et al., 2002; Wang et al., 2009; Wen et al., 2015; Huang et al., 2015; Roy et al., 2018; Li et al., 2019). This offers us an opportunity to further understand the enzymatic-electrochemical cascade reaction and fabricate high-performance bioassays. Despite triphase electrodes have been recently reported using superhydrophobic nanowire arrays, micropillar arrays, anodic alumina membrane, and carbon paper substrates (Chen et al., 2018; Song et al., 2018; Lei et al., 2016; Xu et al., 2016; Cheng et al., 2020; Guan et al., 2019), the complicated fabrication process and the fragile nature of these electrode substrates impede applications in flexible biosensors. Therefore, simple approaches are highly desirable to

* Corresponding author.
** Corresponding author.
E-mail addresses: jzhang2017@suda.edu.cn (J. Zhang), xjfeng@suda.edu.cn (X. Feng).

https://doi.org/10.1016/j.bios.2021.113201
Received 1 January 2021; Received in revised form 13 March 2021; Accepted 23 March 2021
Available online 26 March 2021

construct mechanically stable flexible triphase enzyme electrodes in large scale.

We report here a flexible triphase enzyme electrode (Fig. 1a) where an oxidase-enzyme layer is immobilized on the surface of H_2O_2 electrocatalysts-decorated conductive flexible hydrophobic porous substrate. When the electrode is immersed in an analyte solution, water wets the top enzyme layer but cannot enter the underneath porous flexible substrate. This leads to an air-solid-liquid triphase interfacial microenvironment where oxygen can be supplied rapidly through and from the air phase. In such a case interfacial oxygen level will change from liquid phase dependent (fluctuant and low) to air phase dependent (constant and sufficient). As we know, the factors that influence enzymatic reaction are the amount of enzyme, oxygen level and analyte concentration. For a fixed amount of enzyme, the triphase interfacial enzymatic reaction will be purely governed by the concentration of analyte. Meanwhile, the constant interfacial oxygen level will stabilize the cathodic current contributed from the oxygen reduction reaction, and enable the cathodic measuring of oxidase catalytic product H_2O_2 ($H_2O_2 + 2e^- + 2H^+ \rightarrow 2H_2O$) in biosensor development with minimum interferences caused from oxidizable biologic species. Thus, reliable bioassays can be fabricated based on such a flexible triphase enzyme electrode for accurate analyte detection.

2. Material and methods

Reagent, materials, electrode fabrication methods, characterization and electrochemical measurements can be found in the Supplementary Information.

3. Results and discussion

The flexible triphase enzyme electrode illustrated in Fig. 1a was constructed by choosing a commercially available porous polyvinylidene fluoride (PVDF) membrane as a model substrate. The PVDF membrane has an average pore size of about 1.5 μm and a thickness of about 120 μm (Fig. 1b and inset). Fig. 1c shows the SEM image of a CNTs film immobilized on the porous PVDF membrane that is prepared by vacuum-filtering of a CNTs aqueous dispersion. To further reinforce the adhesion between the CNTs film and the membrane and enhance its surface hydrophobicity, the as-prepared CNTs/PVDF substrate was dipped in a dilute poly-dimethylsiloxane (PDMS) solution (Sylgard 184 in cyclohexane), dried naturally, and cured at 120 °C for 1 h. The PDMS layer has a thickness of about 2.5 nm (Fig. S1). Water contact angle (CA) analysis of the substrate shows that the CA is about 140 ± 2° (Inset of Fig. 1c), indicating an ultra-hydrophobic surface property. After that H_2O_2 electrocatalyst Pt with an average particle diameter of about 450 ± 50 nm was electrodeposited on the CNTs film (Fig. 1d). Finally, a mixed glucose oxidase and chitosan solution was drop-casted onto the Pt decorated CNTs film with an area of 0.25 cm^2 to form the flexible triphase enzyme electrode. The oxidase-chitosan composite layer has a thickness of about 4 μm (Inset of Fig. 1e). Based on such a triphase enzyme electrode architecture (Fig. 1a), oxygen and electrons can transport through the air phase and along the CNTs, respectively, to the enzymatic reaction zone. For comparison, a diphase enzyme electrode was also prepared by using a porous PVDF membrane without PDMS treatment. The detail fabrication process of triphase and diphase enzyme electrodes was shown in Fig. S2.

Rapid oxygen supply capacity is crucial to the performance of oxidase-based bioassays. In order to evaluate the oxygen permeability of CNTs/PVDF electrode substrate with and without hydrophobic PDMS treatment, the kinetics of GOx immobilized on their surface was studied. The formation rate of H_2O_2 ($V_{H_2O_2}$) that is directly related to the oxidase kinetics and the oxygen permeability of electrode substrate were measured by iodometry (Fig. 2a and S3). The corresponding initial formation rates (V_0) of H_2O_2 were calculated via the Beer-Lambert law (Eq. (1)). As shown in Fig. 2b and c, compared with a diphase system where oxygen needed at the reaction zone can only be provided from the liquid phase, the formation rate of H_2O_2 at the triphase system was greatly increased. Because the dose-dependent plot is consistent with the unique property of the Michaelis–Menten kinetic mechanism (Laviron, 1979), the parameters of the enzymatic reaction kinetics were also determined. The maximum velocity (V_{max}) of triphase and diphase systems can be determined to be 0.026 μmol/min and 0.0023 μmol/min from Equation (2), respectively. By integrating the V_{max} value into

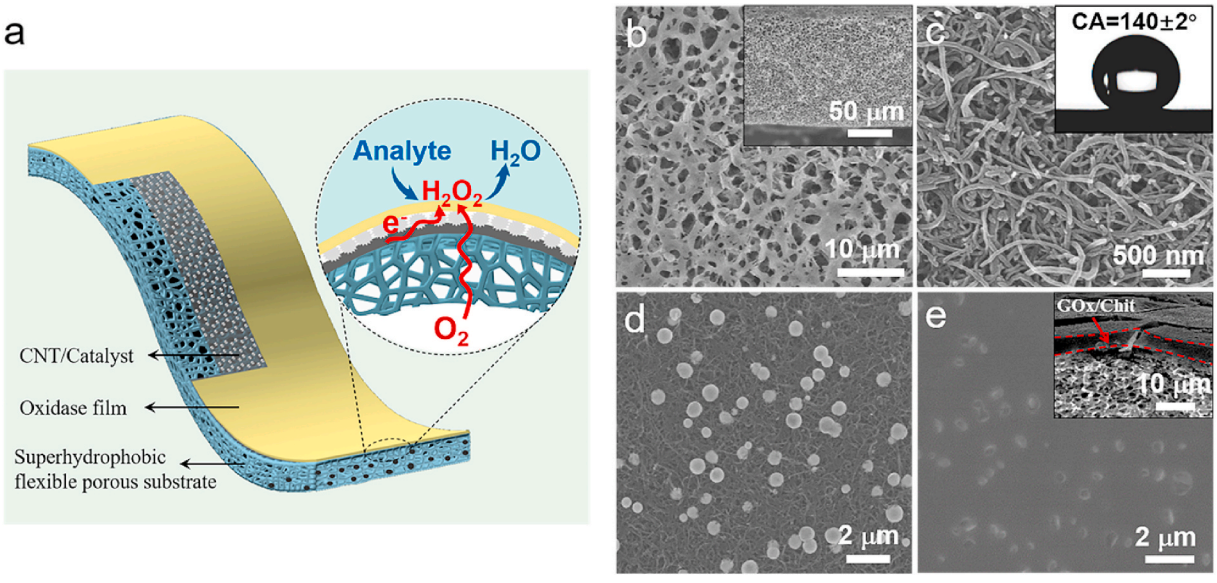

Fig. 1. a) Schematic drawing of the flexible triphase enzyme electrode. The electrode consists of a hydrophobic flexible porous substrate, a H_2O_2 electrocatalyst modified carbon nanotubes (CNTs) film, and a top enzyme layer. The inset shows an enlarged view of the air-liquid-solid triphase bio electrochemical cascade reaction zone, where air-dependent (constant) interfacial oxygen level can be obtained. b) Scanning electron microscopy (SEM) top view of a flexible porous polyvinylidene fluoride (PVDF) substrate with a pore diameter of about 1.5 μm. The inset shows a SEM side view of the porous substrate. c) SEM image of the CNTs film on a porous substrate; the inset shows a water droplet placed on the CNTs/PVDF substrate after hydrophobic treatment using poly-dimethylsiloxane (PDMS); the inset shows a water droplet placed on the electrode substrate with a CA of about 140 ± 2°. d) SEM image of the H_2O_2 electrocatalysts (Pt) electrodeposited on the CNTs film. e) SEM top view of the glucose oxidase/chitosan layer electrode; the inset shows a SEM side view of the oxidase enzyme electrode.

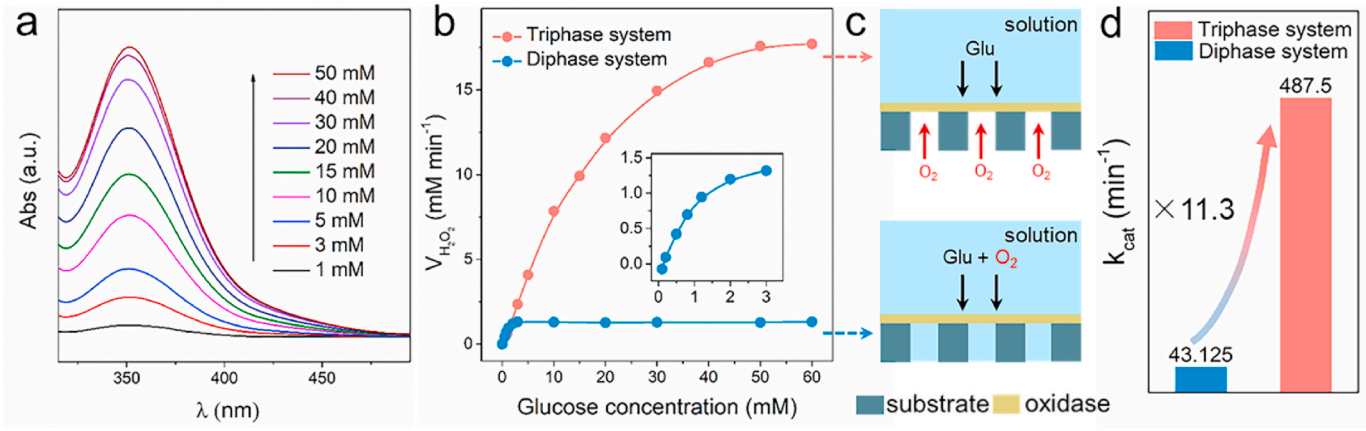

Fig. 2. a) Absorption (Abs.)spectra of oxidase enzymatic product H_2O_2 at different glucose (Glu) concentration using the triphase system. b) H_2O_2 production rate as a function of glucose concentration using triphase and diphase systems. c) Schematic illustrations of the triphase and diphase oxidase catalytic reaction systems. d) Apparent catalytic constant (k_{cat}) of GOx based on diphase and triphase systems.

equation (3), the apparent oxidase catalytic constant (k_{cat}) at the triphase electrode can be calculated to be 487.5 min^{-1}, a value of 11.3-fold higher than that obtained using a diphase electrode (43.1 min^{-1}) as shown in Fig. 2d. These results confirm that the hydrophobic PDMS treatment did not block the oxygen transport pathway, but instead endowed the porous CNTs/PVDF electrode substrate with a much higher oxygen permeability.

$$A = kbc \tag{1}$$

$$V_0 = \frac{V_{max} \cdot [S]}{K_m + [S]} \tag{2}$$

$$k_{cat} = \frac{V_{max}}{[E]} \tag{3}$$

The performance of the triphase and diphase enzyme electrodes was then evaluated by using as the cathode. We first investigated the effect of oxygen contents in analyte solution on cathodic current of the enzyme electrodes. Before the experiment, the oxygen content in phosphate-buffered saline (PBS) solution was changed by purging the electrolyte with nitrogen. For a diphase electrode where interfacial oxygen can only be obtained from solution, the cathodic current keeps increasing with oxygen concentration as shown in Fig. 3a (blue columns) and Fig. S4a

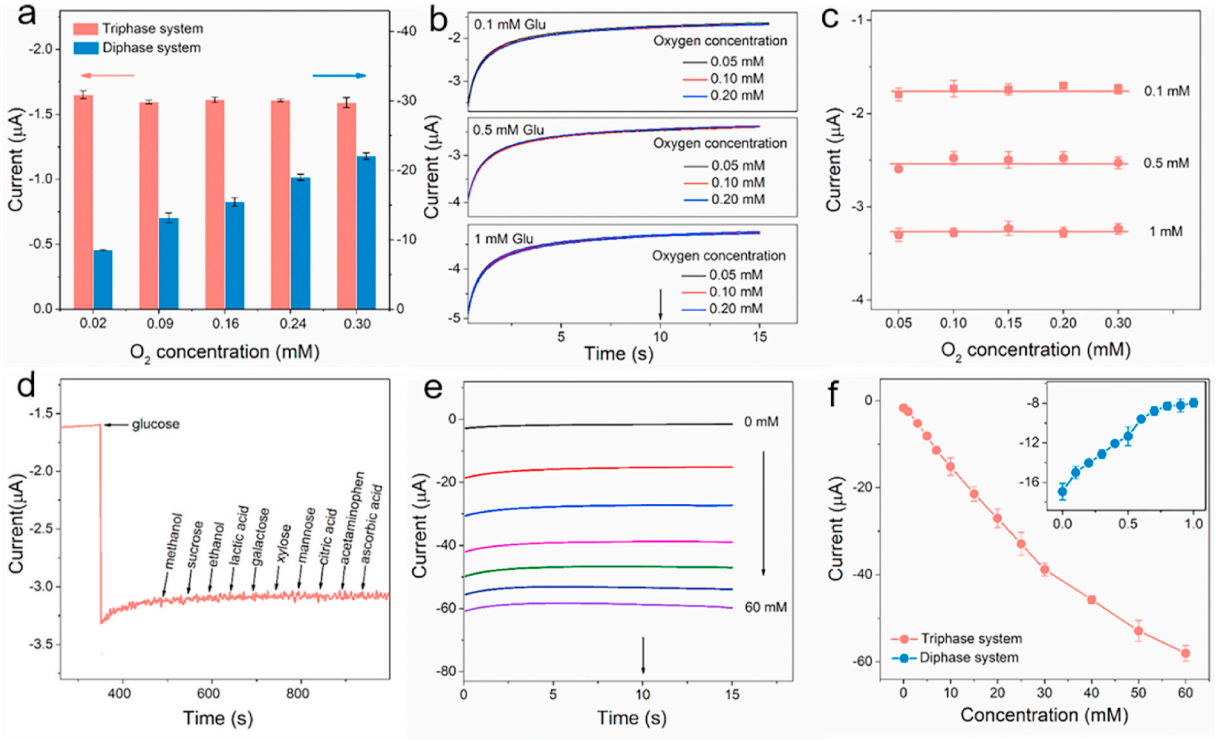

Fig. 3. a) Background currents of the diphase and triphase enzyme electrodes in blank PBS solution with different oxygen contents at 0 V versus (vs) Ag/AgCl. b) Amperometric i-t curves using flexible triphase enzyme electrode in 0.1, 0.5 and 1 mM glucose solution with various oxygen contents. c) Corresponding calibration plot derived from (b) at 10 s. Cathodic response of the flexible triphase biosensors when operated in 0.1, 0.5, and 1 mM glucose solutions with various oxygen levels. d) Cathodic current responses for 1 mM glucose after successive addition of 0.1 mM interferents using the triphase enzyme electrode. e) Amperometric i-t curves corresponding to the triphase enzyme electrode with glucose concentrations up to 60 mM. f) Corresponding calibration plot derived from (a) at 10 s and the inset for diphase one. An upper linear detection limit of ~ 30 mM is observed—this is 40 times higher than that from a diphase system (~0.7 mM).

(Supporting information). This can be attributed to the oxygen reduction reaction. The variable cathodic currents caused by oxygen level fluctuations will compromise the cathodic measurement of enzymatic product H_2O_2 and limit its practical application in biosensor development. In contrast, for the triphase electrode system, negligible influence of oxygen level fluctuations in the electrolyte on the cathodic current response was observed (Fig. 3a, red columns and Fig. S4b), suggesting that oxygen level at the triphase reaction zone is dependent on air phase (constant). The oxygen level fluctuation-tolerant performance of the triphase enzyme electrode enables the development of biosensor using the principle of cathodic measurement of the enzymatic product of H_2O_2.

The constant oxygen level at the triphase reaction zone can also stabilize the oxidase kinetics and the formation rate of H_2O_2. This consequently increases the detection reliability. Fig. 3b and c show that the current response of flexible triphase enzyme electrode toward 0.1, 0.5, and 1 mM glucose under different oxygen concentrations is constant. Conversely, for a diphase system, the 1 mM glucose response current gradually increases as the oxygen content increases (Fig. S5). The results show that the current output of the triphase enzyme electrode toward a fixed glucose concentration is insensitive to the dissolved oxygen content variety due to the stable interfacial oxygen level and oxidase kinetics. This offers us a good opportunity to eliminate interferences from many oxidizable species in biofluids during common H_2O_2 anodic reaction, leading to improved detection selectivity. Fig. 3d shows negligible current output variation after 0.1 mM methanol, sucrose, ethanol, lactic acid, galactose, xylose, mannose, citric acid, acetamido phenol (AP), and ascorbic acid (AA) were successively added into 1 mM glucose (a model analyte), suggesting a high detection selectivity of the triphase enzyme electrode-based biosensor.

The triphase enzyme electrode allows rapid diffusion of oxygen through the air phase to the oxidase catalytic reaction zone, which will increase the interface oxygen level, enhance the oxidase kinetics and broaden the linear detection range. Fig. 3e shows that the current response of triphase enzyme electrode increases with glucose content up to a value of about 60 mM. Cathodic current response versus glucose concentration (Fig. 3f) shows that the triphase electrode displays a linear detection range up to about 30 mM (red line). In contrast, for the diphase electrode (inset of Fig. 3f and Fig. S6), a decrease in apparent cathodic current was observed as the glucose concentration increases. This is because the cathodic current increase caused by the enzymatic product H_2O_2 is counteracted by the current decrease resulting from oxygen consumption due to the oxidase catalytic reaction. Thus, a significantly low upper detection limit is obtained (~0.7 mM) when a diphase enzyme electrode was used.

Fig. S7 shows the response of triphase enzyme electrode in the presence of glucose with a concentration less than 1 mM; this suggests that the triphase biosensor also has a good linearity at low analyte level with a detection limit as low as 5 μM. Repeated measurements using one flexible triphase biosensor in 1 mM glucose solution were also conducted, and the relative standard deviation is about 2.38% (Fig. S8). Such flexible triphase enzyme electrodes are applicable to other oxidase-based biosensors. We further measured sucrose and lactic acid levels by using their corresponding oxidase-based triphase electrodes. Fig. S9 shows that the cathodic current increases with sucrose and lactic acid concentration; the linear dynamic range of the triphase enzyme electrode-based biosensors is 30 and 25 times wider than those obtained using conventional diphase enzyme electrode, respectively (insets of Figs. S9a and b), suggesting a good application universality of the triphase enzyme electrode.

Flexible biosensors require high mechanical durability and stability. We further studied the relationship between the background current and the number of bending cycles with a bending radius of 0.5 cm (Fig. S10a). Fig. S10b and Fig. S11a show that negligible background current change was observed after the electrode being bent 600 times. Next, we studied the bending effect of the electrode on the glucose detection performance. Fig. S10c and Figs. S11b and c show that the response currents of the enzyme electrode at 5 mM and 10 mM glucose remain almost constant even after 600 time bending cycles, suggesting a good mechanical stability of the triphase enzyme electrode.

Excellent breathability is another important feature of wearable electronics (Xu et al., 2019). The breathability of the flexible diphase bioelectronics has been limited due to the common use of planar plastic or elastomer substrates. Our triphase enzyme electrode exhibits excellent water vapor permeability. As shown in Fig. S12, in this experiment, the triphase electrode was adhered to the opening of a bottle filled with water. The permeability was evaluated by monitoring the weight change of the water. The weight loss of water with the triphase electrode changed similarly to the opening bottle. In contrast, for commonly used electrode substrates, such as PET film, the weight of the bottle was barely reduced after 8 days. This result shows the high gas permeability of the triphase electrode; it effectively supports its application to wearable devices requiring long-term skin contact.

4. Conclusion

In summary, we have constructed a flexible enzyme electrode with an air-liquid-solid triphase interface based on superhydrophobic CNTs film/porous PVDF membrane. Unlike the traditional diphase system with low and fluctuant oxygen level, the interface oxygen level is air phase dependent in the triphase system. With a constant and high interfacial oxygen level, the demonstrated enzyme electrode stabilized and enhanced the oxidase kinetics, and enabled the cathodic measurement of enzymatic product H_2O_2 in biosensor development. The investigations of the flexible triphase enzyme electrode allow for determination of glucose, lactic acid, and sucrose with a wide linear range, accuracy, and selectivity. In the future, this oxygen and biologic interferent-tolerant flexible enzyme electrode can be integrated with reference and counter electrodes into a portable biosensor, providing a reliable monitoring platform for non-invasive physiological biomarkers assay in perspiration, saliva, tears and interstitial fluid.

Author contributions

Xinjian Feng supervised the project. Haili Wang designed the devices and completed the experiments. Jun Zhang and Zhaohong Wang conducted SEM and CA characterizations. Jun Zhang and Haili Wang drafted the manuscript. Jun Zhang and Dandan Wang discussed the data. All authors revised the manuscript.

Declaration of interest

The authors declare that they have no known competing financial interests or personal relationships that could have appeared to influence the work reported in this paper.

CRediT authorship contribution statement

Haili Wang: Methodology, Writing – original draft, Data curation. **Jun Zhang:** Writing – original draft, Data curation. **Dandan Wang:** Writing – original draft, Data curation. **Zhaohong Wang:** Methodology. **Yangru Chen:** Methodology. **Xinjian Feng:** Supervision, Writing – review & editing.

Declaration of competing interest

The authors declare that they have no known competing financial interests or personal relationships that could have appeared to influence the work reported in this paper.

Acknowledgments

This research was financially supported by the National Key Research and Development Program of China (2019YFA0709200) and the National Natural Science Foundation of China (21988102, 51772198 and 21975171).

Appendix A. Supplementary data

Supplementary data to this article can be found online at https://doi.org/10.1016/j.bios.2021.113201.

References

Barthlott, W., Neinhuis, C., 1997. Planta 202 (1), 1–8.
Chen, L., Sheng, X., Wang, D., Liu, J., Sun, R., Jiang, L., Feng, X., 2018. Adv. Funct. Mater. 28, 1801483.
Chen, D., Wang, C., Chen, W., Chen, Y., Zhang, J.X., 2015. Biosens. Bioelectron. 74, 1047–1052.
Cheng, Q., Zhang, J., Wang, H., Wang, D., Feng, X., Jiang, L., 2020. Adv. Mater. Interfaces 7, 1902172.
Evans, S.A.G., Elliott, J.M., Andrews, L.M., Bartlett, P.N., Doyle, P.J., Denuault, G., 2002. Anal. Chem. 74 (6), 1322–1326.
Feng, L., Li, S.H., Li, Y.S., Li, H.J., Zhang, L.J., Zhai, J., Song, Y.L., Liu, B.Q., Jiang, L., Zhu, D.B., 2002. Adv. Mater. 14 (24), 1857–1860.
Gao, W., Emaminejad, S., Nyein, H.Y.Y., Challa, S., Chen, K., Peck, A., Fahad, H.M., Ota, H., Shiraki, H., Kiriya, D., Lien, D.H., Brooks, G.A., Davis, R.W., Javey, A., 2016. Nature 529 (7587), 509–514.
Guan, F., Zhang, J., Tang, H., Chen, L., Feng, X., 2019. Nanoscale Horiz. 4 (1), 231–235.
Guilbault, G.G., Lubrano, G.J., 1973. Anal. Chim. Acta 64 (3), 439–455.
Hrapovic, S., Liu, Y., Male, K.B., Luong, J.H.T., 2004. Anal. Chem. 76 (4), 1083–1088.
Huang, J.Y., Li, S.H., Ge, M.Z., Wang, L.N., Xing, T.L., Chen, G.Q., Liu, X.F., Al-Deyab, S. S., Zhang, K.Q., Chen, T., Lai, Y.K., 2015. J. Mater. Chem. A3 (6), 2825–2832.
Imani, S., Bandodkar, A.J., Mohan, A.M., Kumar, R., Yu, S., Wang, J., Mercier, P.P., 2016. Nat. Commun. 7, 11650.
Kim, J., Kim, M., Lee, M.S., Kim, K., Ji, S., Kim, Y.T., Park, J., Na, K., Bae, K.H., Kyun Kim, H., Bien, F., Young Lee, C., Park, J.U., 2017. Nat. Commun. 8, 14997.
Kim, J., Jeerapan, I., Sempionatto, J.R., Barfidokht, A., Mishra, R.K., Campbell, A.S., Hubble, L.J., Wang, J., 2018. Acc. Chem. Res. 51 (11), 2820–2828.
Kim, J., Campbell, A.S., de Avila, B.E., Wang, J., 2019. Nat. Biotechnol. 37 (4), 389–406.
Kumar, P., Narwal, V., Jaiwal, R., Pundir, C.S., 2018. Biosens. Bioelectron. 122, 140–146.
Lad, U., Kale, G.M., Bryaskova, R., 2014. J. Electrochem. Soc. 161 (5), B98–B101.
Laviron, E., 1979. J. Electroanal. Chem. 101, 19–28.
Lee, H.B., Meeseepong, M., Trung, T.Q., Kim, B.Y., Lee, N.E., 2020. Biosens. Bioelectron. 156, 112133.
Lei, Y., Sun, R., Zhang, X., Feng, X., Jiang, L., 2016. Adv. Mater. 28 (7), 1477–1481.
Li, L., Wang, Y., Pan, L., Shi, Y., Cheng, W., Shi, Y., Yu, G., 2015. Nano Lett. 15 (2), 1146–1151.
Li, J., Hou, Y., Liu, Y., Hao, C., Li, M., Chaudhury, M.K., Yao, S., Wang, Z., 2016. Nat. Phys. 12 (6), 606–612.
Li, Z., Cao, M., Li, P., Zhao, Y., Bai, H., Wu, Y., Jiang, L., 2019. Matter 1 (3), 661–673.
Lu, Y., Sathasivam, S., Song, J.L., Crick, C.R., Carmalt, C.J., Parkin, I.P., 2015. Science 347 (6226), 1132–1135.
Lu, Z., Xu, W., Ma, J., Li, Y., Sun, X., Jiang, L., 2016. Adv. Mater. 28 (33), 7155–7161.
Mi, L., Yu, J., He, F., Jiang, L., Wu, Y., Yang, L., Han, X., Li, Y., Liu, A., Wei, W., Zhang, Y., Tian, Y., Liu, S., Jiang, L., 2017. J. Am. Chem. Soc. 139 (30), 10441–10446.
Roy, P., Kisslinger, R., Farsinezhad, S., Mahdi, N., Bhatnagar, A., Hosseini, A., Bu, L.T., Hua, W.D., Wiltshire, B.D., Eisenhawer, A., Kar, P., Shankar, K., 2018. Chem. Eng. J. 351, 482–489.
Sheng, X., Liu, Z., Zeng, R., Chen, L., Feng, X., Jiang, L., 2017. J. Am. Chem. Soc. 139 (36), 12402–12405.
Song, Z., Xu, C., Sheng, X., Feng, X., Jiang, L., 2018. Adv. Mater. 30, 1701473.
Wang, J., Zheng, Y., Nie, F.-Q., Zhai, J., Jiang, L., 2009. Langmuir 25 (24), 14129–14134.
Wang, S., Wu, Y., Kan, X., Su, B., Jiang, L., 2014. Adv. Funct. Mater. 24 (44), 7007–7013.
Wen, L., Tian, Y., Jiang, L., 2015. Angew. Chem. Int. Ed. 54 (11), 3387–3399.
Wilson, G.S., Hu, Y., 2000. Chem. Rev. 100 (7), 2693–2704.
Xu, C., Song, Z., Xiang, Q., Jin, J., Feng, X., 2016. Nanoscale 8 (14), 7391–7395.
Xu, J.-L., Liu, Y.-H., Gao, X., Shen, S., Wang, S.-D., 2019. Energy Stor. Mater. 22, 402–409.
Yang, Y., Gao, W., 2019. Chem. Soc. Rev. 48 (6), 1465–1491.
Yao, H., Shum, A.J., Cowan, M., Lähdesmäki, I., Parviz, B.A., 2011. Biosens. Bioelectron. 26 (7), 3290–3296.
Yohe, S.T., Colson, Y.L., Grinstaff, M.W., 2012. J. Am. Chem. Soc. 134 (4), 2016–2019.
Yoon, J., Lee, S.N., Shin, M.K., Kim, H.W., Choi, H.K., Lee, T., Choi, J.W., 2019. Biosens. Bioelectron. 140, 111343.
Zhan, S., Pan, Y., Gao, Z.F., Lou, X., Xia, F., 2018. TrAC Trends Anal. Chem. (Reference Ed.) 108, 183–194.
Zhang, J., Sheng, X., Jin, J., Feng, X., Jiang, L., 2017. Nano Res. 10 (9), 2998–3004.
Zhang, J., Sheng, X., Ding, Z., Wang, H., Feng, L., Zhang, X., Wen, L., Jiang, L., Feng, X., 2020. Sci. Bull. 66 (2), 164–169.
Zhou, H., Sheng, X., Xiao, J., Ding, Z., Wang, D., Zhang, X., Liu, J., Wu, R., Feng, X., Jiang, L., 2020. J. Am. Chem. Soc. 142 (6), 2738–2743.